Optical implementation of multifocal programmable lens with single and multiple axes

2011 J. Phys.: Conf. Ser. 274 012050

(http://iopscience.iop.org/1742-6596/274/1/012050)

Journal of Physics: Conference Series **274** (2011) 012050 doi:10.1088/1742-6596/274/1/012050

Optical implementation of multifocal programmable lens with single and multiple axes.

Lenny A. Romero, María S. Millán, and Elisabet Pérez-Cabré
Optics & Optometry Dep. Technical University of Catalonia
Violinista Vellsolà 37, 08222 Terrassa, SPAIN

E-mail: lenny.alexandra.romero@upc.edu

Abstract. In this work we analyse the generation of a diffractive optical element (DOE) consisting of a multifocal Fresnel lens by means of an LCoS (liquid cristal on silicon) spatial light modulator (SLM). The multifocal lens is composed of a set of lenses of different focal length that share a common optical axis (coaxial combination) or have different axes in parallel (multi-axis combination). For both configurations, we present several ways to combine the phase distributions for three lenses with different focal lengths (f_1, f_2, f_3), into a single-phase distribution addressed to the SLM. Numerical simulations were carried out along with the experimental analysis to corroborate the results.

1. Introduction

Programmable diffractive lenses reproduced using spatial light modulators (SLM)[1-3] are of great importance in building image-forming optical systems. This is mainly due to the advantages gained in versatility and the use of less number of elements because the SLM allows the combination of different diffractive optical elements (DOEs) into one, such as Fresnel monofocal and multifocal lenses[4,5,6].

Several studies have examined the combination of diffractive lenses in one device[5-9]. Different schemes exist, such as multifunction coding methods or spatial multiplexing methods. Iemmi et al.[7] propose spatially multiplexed lenses with nearby focal lengths to increase the depth of focus. Márquez et al.[8] propose a multiplexed diffractive lens that is able to provide focal lengths for several wavelengths simultaneously. Otón et al.[9,10] propose to compensate chromatic aberration by means of a multiplexed lens designed with a common focal length for different wavelengths, and a multicolour filter that makes each sublens work almost monochromatically.

In this work we introduce four coding methods for merging the phase distributions of three Fresnel lenses, (f_1, f_2, f_3), of different focal length into a single-phase distribution. The resulting phase is implemented experimentally via an LCoS SLM (HEO 1080P Holoeye)[11] previously calibrated and characterised[12]. The combination of lenses is arranged for two configurations: coaxial and multiaxis. In the former, all lenses have a common optical axis, whereas in the latter the lenses have parallel separated axes. In section 2, we describe the main features of such lenses by taking into account the actual technical constraints given by the SLM specifications. In section 3 we describe different

methods for spatial encoding the three combined lenses. Finally, in section 4 we show numerical simulations and experimental results with an extended test-object for each coding method.

2. Spatial discretization of the continuos Fresnel lens function

A lens with focal length f can be described as an optical element that introduces a quadratic phase onto an incident wavefront λ. Using one-dimensional notation for simplicity, we can express this phase distribution by the continuous function:

$$l(x,f)=\exp\left\{-j\frac{\pi}{\lambda f}\left(x_0^2\right)\right\}. \tag{1}$$

When the phase distribution of Eq (1) is addressed to a SLM, the pixelated structure of the modulator is responsible for a spatial discretization of the phase distribution displayed in the SLM. This discrete phase distribution can be written as:

$$l(p,f)=\exp\left\{-j\frac{\pi}{\lambda f}\frac{L^2}{N_l^2}p\right\}, p\in\left[-\frac{N_l}{2}+1,\frac{N_l}{2}\right], \tag{2}$$

where L is the diameter of the lens aperture that corresponds to a given number of pixels N_l.

The discretization of (1) implies an adequate sampling of the exponential function; i.e. the Nyquist sampling condition needs to be fulfilled. This condition indicates that the phase shift between two neighbour pixels of Eq.(2) where the phase oscillation is faster, that is, at the border of the lens aperture, $p=\left(N_l/2-1\right),\left(N_l/2\right)$, has to be lower than or equal to π. Therefore, there is a minimum value recommended for the focal length of the lens generated by using an SLM. Assuming that $L=N_l\Delta$ where Δ is the square pixel pitch, we can define a reference focal length[5], f_{ref}, as

$$f_{ref}=\frac{N_l}{\lambda}\Delta^2. \tag{3}$$

In this work, we have used a spatial light modulator as reflective display based on the parallel aligned LCoS technology (HEO 1080P) manufactured by Holoeye. It has a HDTV resolution of 1920 x 1080 pixels in a 15.36 mm x 8.64 mm size array, with a square pixel pitch of 8.0 μm, 87% fill factor and a number of electrically addressable levels of 8-bit. The SLM works in a phase-only modulation regime and it has a modulation range [0, 2π] discretised into 256 gray levels. A $\lambda=633\,nm$ is used in all cases.

3. Spatial encoding the multifocal lens

To combine multiple lenses in a single phase distribution, two different encoding methods are used: lenses are either coded by rows or randomly. And two configurations are considered: the lenses share a common optical axis (coaxial configuration) or have different parallel axes (multi-axis configuration). In all cases, three sublenses l_1, l_2, l_3 with respective focal lengths f_1, f_2, f_3, are combined. All the focal lengths used in these experiments are greater than f_{ref}. The focal lengths for l_1, l_2, l_3 sublenses are f_1= 35 cm, f_2= 25cm and f_3= 30 cm, respectively, where f_2 is the closest to the f_{ref} of the Eq. 3. The following subsections describe the procedure carried out for every configuration. Figures 1-4 show the resulting phase distributions represented in grey levels that are sent to the modulator.

3.1. Multifocal lens coded by rows

This method consists of subdividing the aperture of the modulator in horizontal lines of pixels and assigning each row of the modulator to one sublens sequentially. The resulting phase distribution is then built row by row until completing the SLM aperture.

3.1.1. Coaxial configuration.

The codification by rows is applied to display a multifocal lens in coaxial configuration where the optical axes of the three sublenses l_1, l_2, l_3 coincide. Figure 1(a) shows a grey level representation of the phase distribution of the multifocal lens by this method.

3.1.2. Multi-axis configuration.

In this configuration the optical axes of the three sublenses are parallel between them. Using the coding by rows method, we design a multifocal lens in multi-axis configuration. The optical centres of l_1 and l_3 sublenses have been displaced horizontally a certain amount in opposite direction from the centre of l_2. Each lens can be described as follows: $l_1\left(x_0 + x_d, f_1\right), l_2\left(x_0, f_2\right), l_3\left(x_0 - x_d, f_3\right)$. Figure 1(b) shows a grey level representation of the phase distribution of the multifocal lens with multi-axis configuration.

3.2. Multifocal lens randomly coded

In this method the phase of the lenses is randomly distributed among the pixels. Each pixel (x,y) of the SLM's aperture is assigned a value of k between 0 and 1 randomly. If $k \leq (1/3)$, the pixel represents the phase of $l_1(x,y)$. If $(1/3) < k \leq (2/3)$, the pixel represents the phase of $l_2(x,y)$ and finally, if $(2/3) < k$ the pixel represents the phase of $l_3(x,y)$. Using this method we have designed a multifocal lens in coaxial and multi-axis configuration.

3.2.1. Coaxial configuration.

Figure 1(c) shows a grey level representation of the phase distribution of the multifocal lens with coaxial configuration. Again, the optical axes of the three sublenses coincide.

3.2.2. Multi-axis configuration.

Figure 1(d) shows a grey level representation of the phase distribution of the multifocal lens with multiaxis configuration.

4. Numerical and experimental results

Let us consider a small portion of the test USAF as an extended object at infinity. It is illuminated by a plane wave of λ=633 nm. The three sublenses form the image at different distances in the image space. Displacing conveniently the CCD sensor the images were captured.

For all the cases mentioned in Section 3, numerical simulations were carried out, along with experimental results. Initially, we show the results obtained from the numerical simulations, followed by the experimental results and finally we summarize and discuss the behaviour for each method and configuration

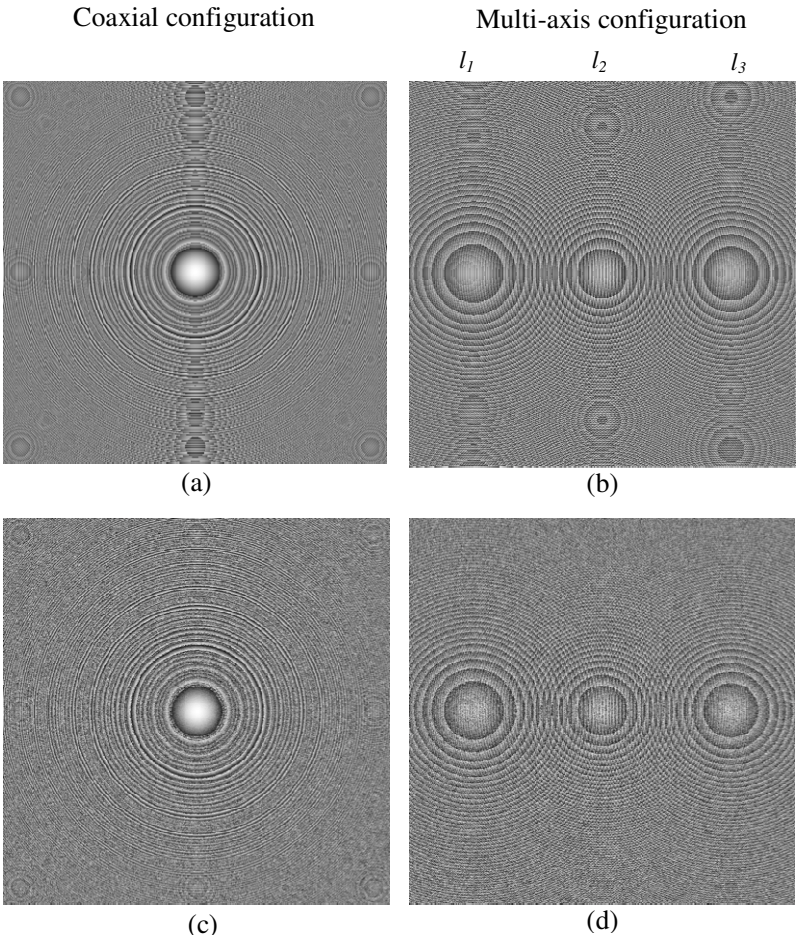

Figure 1. Phase distributions for three lenses (l_1, l_2, l_3) of different focal length in coaxial and multi-axis configuration. (a) and (b) Multifocal lens coded by rows, (c) and (d) multifocal lens randomly coded.

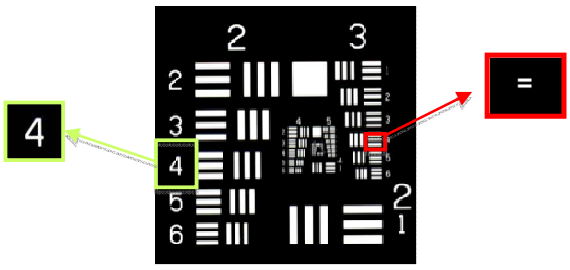

Figure 2. The boxes show two small portions of the USAF test used as extended objects. The object highlighted on the left-hand side (number four) was used for experimental analysis, while the one on the opposite (double bar) side for numerical simulations.

4.1. Numerical simulation results

In this subsection we present the numerical simulation results obtained by means of Fresnel propagation. In Fig. 3 we show the results in the image plane for the multi-focal lens coded by rows, where Fig. 3(a) corresponds to the coaxial configuration and Fig. 3(b) to the multi-axis. In the coaxial configuration the three images overlap due to the fact that the optical axes of the three sublenses coincide. In the multi-axis configuration the optical axes of the three sublenses are parallel. If the output plane is brought to focus the image formed by one sublens, the other two images will be defocused. When the three sublenses are regularly encoded by rows on the SLM, vertical repetitions of the image appear due to the multiple diffraction orders introduced by the coding procedure.

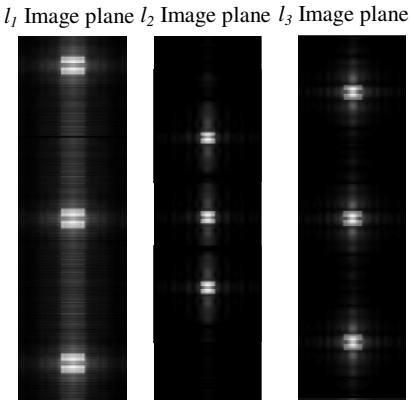

(a)

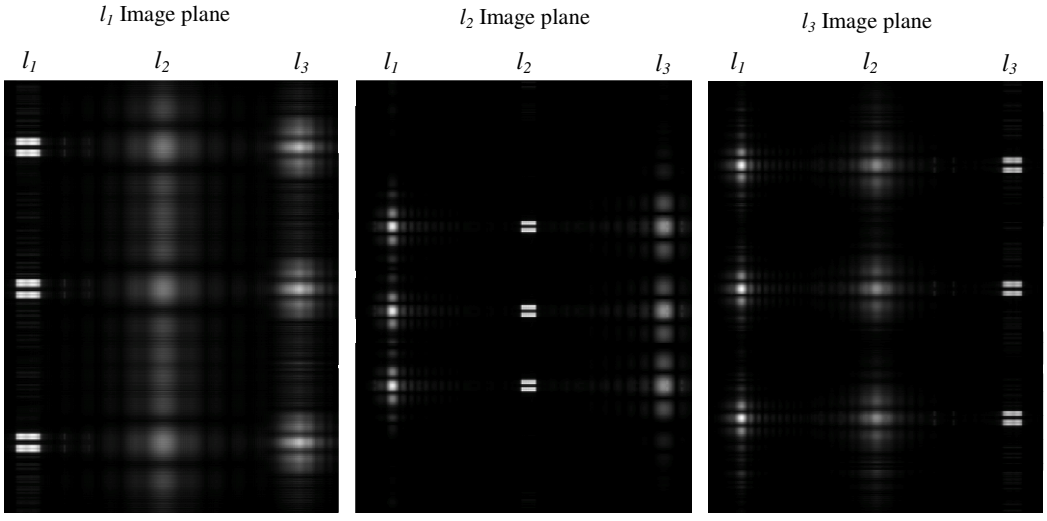

(b)

Figure 3. Simulated image planes of the lenses coded by rows in (a) coaxial and (b) multi-axis configurations; l_1 (f_1= 35 cm), l_2 (f_2 = 25 cm), l_3 (f_3 = 30 cm).

Figure 4 shows the intensity distribution of the three different image planes for (a) coaxial and (b) multi-axis configuration, using the randomly coded multi-focal lens. In each image plane a coaxial

superposition of three images is observed, while one of them is in focus the other two appear defocused. The multi-axis configuration permits to spatially separate these images. Differently from the multilens coded by rows, no additional diffraction orders appear in the image planes.

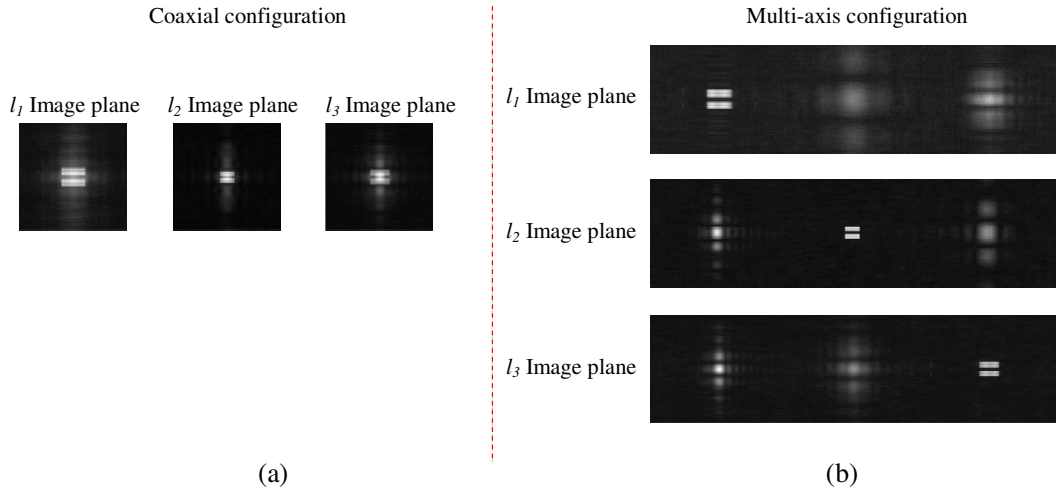

Figure 4. Simulated image planes of the lenses randomly coded in (a) coaxial and (b) multi-axis configurations; l_1 (f_1= 35 cm), l_2 (f_2 = 25 cm), l_3 (f_3 = 30 cm).

4.2. Experimental results

Here we present the experimental results obtained in an optical bench. The images were captured displacing conveniently the CCD sensor. Analogous to the numerical simulation results, in Fig. 5 we show the results in the image plane for the multi-focal lens coded by rows. Figure 5 and 6 correspond to the coaxial and multi-axis configuration, respectively. We verified the correspondence between the numerical and experimental results, although, only the central zero-order image is shown because the images of the higher orders were outside the field of the CCD.

Similarly to the numerical simulations, we observe in Fig. 5 the overlapping of the three images in the coaxial configuration. To make the overlapping more evident, we also show the intensity profiles corresponding to a row of the image. Note that each profile indicates that there is an energy contribution due to the overlapping of defocused images that increases the energy background and entails a loss of contrast in the resulting image.

In Fig. 6 we show the results obtained for the multi-axis configuration coded by rows. Intensity profiles are also shown to enhance the visualization of the results. In this case, the focused images do not share the same axis with the defocused counterparts, and thus, an improved contrast is obtained.

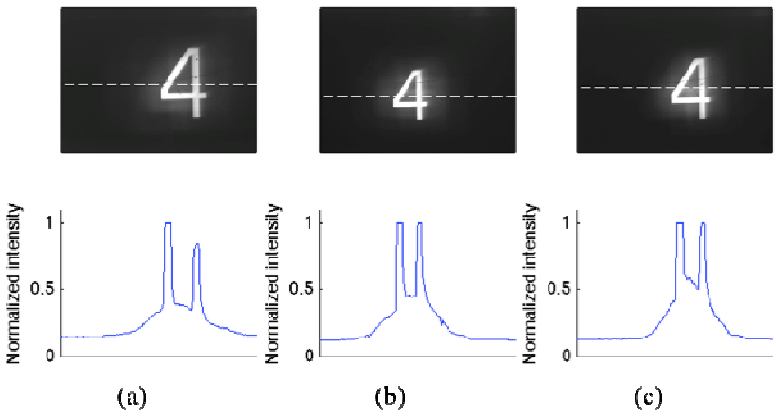

Figure 5. Experimental image plane of the lenses coded by rows in coaxial configuration; below each image, a profile represents the normalized intensity values along the image row marked with a dashed line. (a) l_1 (f_1= 35 cm), (b) l_2 (f_2 = 25 cm) and (c) l_3 (f_3 = 30 cm).

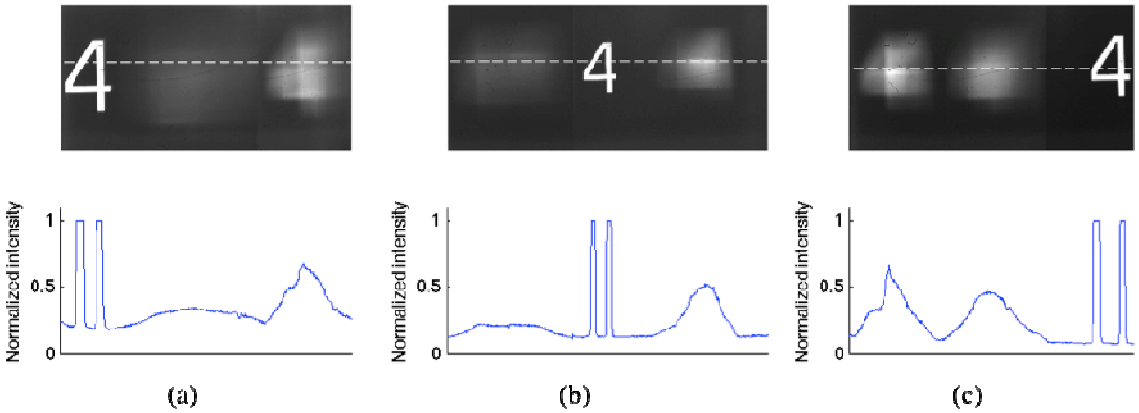

Figure 6. Experimental image plane coded by rows in multi-axis configuration; below each image, a profile represents the normalized intensity values along the image row marked with a dashed line. (a) l_1 (f_1= 35 cm), (b) l_2 (f_2 = 25 cm) (c) l_3 (f_3 = 30 cm).

Figures 7 and 8 show the intensity distribution of the three different image planes for the coaxial and multi-axis randomly coded multifocal lenses, respectively. As expected, the overlapping is present for the coaxial configuration. The multi-axis configuration is not affected by this overlapping and enables a more contrasted focused image in each image plane. We also show intensity profiles for this set of images to better appreciate the effect of overlapping This method has advantages because it does not generate multiorder replicas of the image.

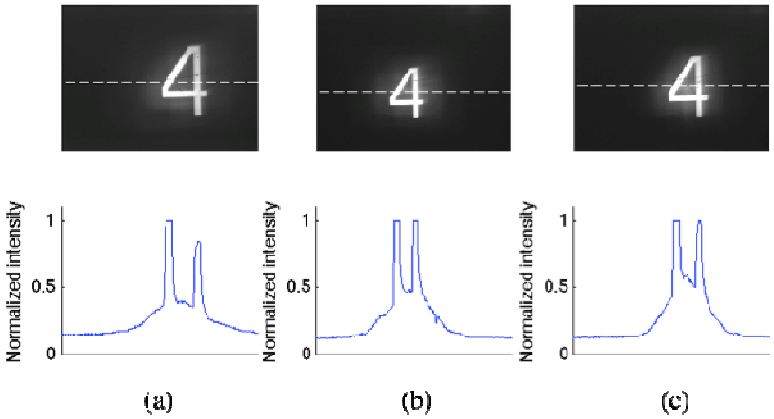

Figure 7. Experimental image plane of the lenses randomly coded in coaxial configuration; below each image, a profile represents the normalized intensity values along the image row marked with a dashed line.(a) l_1 (f_1= 35 cm), (b) l_2 (f_2 = 25 cm) (c) l_3 (f_3 = 30 cm).

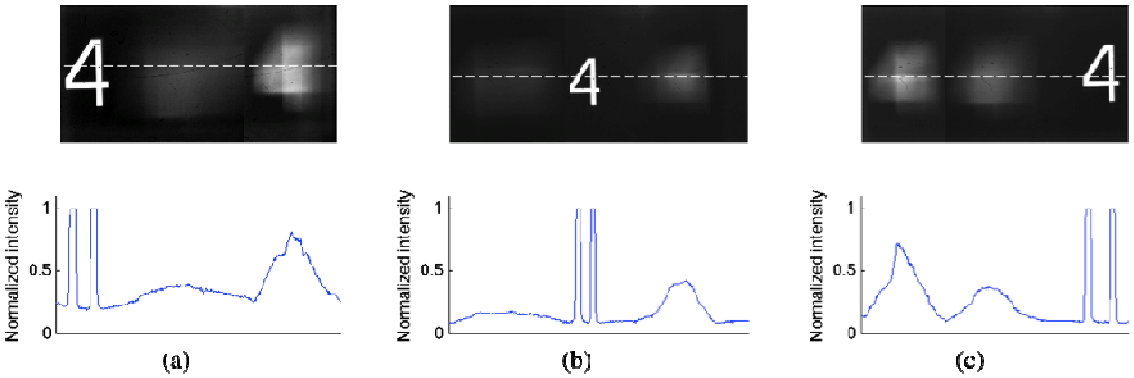

Figure 8. Experimental image plane of the lenses randomly coded multi-axis configuration; below each image, a profile represents the normalized intensity values along the image row marked with a dashed line.(a) l_1 (f_1= 35 cm), (b) l_2 (f_2 = 25 cm) (c) l_3 (f_3 = 30 cm).

5. Conclusions

We have studied the generation of a DOE that consists of a combination of three sublenses with different focal lengths and with optical axes in either coaxial or multi-axis configuration. In addition, for both configurations, we have used two methods for the spatial encoding of the phase distribution of the composite system: a multilens coded by rows, and a multilens randomly coded.

We found the experimental results to be consistent with the numerical simulations carried out for each configuration. The experimental results bring out the fact that the multi-axis configuration is characterized by providing a good contrast in the images planes that are in focus. On the other hand, the coaxial configuration images with poor contrast due to the image overlapping on the same axis.

Regarding the encoding methods, we have verified that the row encoding method generates multiorder image replicas given by the repeating pattern introduced by the codification, whereas the random encoding method has not this disadvantageous effect.

6. References

[1] V. Laude 1998 *Opt. Commun.* **153** 134–52
[2] J. A. Davis, D.M Cottrell, R.A. Lilly, S. W. Connely 1989 *Opt. Lett.* **14(9)** 420-22
[3] S. Serati, K. Bauchet 1999 *Laser Focus World* 229-33
[4] P. Ambs, L. Bigué, E. Hueber 2004 *Proc. SPIE* **5518** 92-103
[5] J. Otón, M. S. Millán, E. Pérez-Cabré 2005 *Opt. Pura Apl.* **38**, 47-56
[6] C. Iemmi, J. Campos, J. C. Escalera, O. López-Coronado, R. Gimeno, M. J. Yzuel 2006 *Opt. Express* **14** 10207-19
[7] L. A. Romero, M. S. Millán, E. Pérez-Cabré 2010 *Opt. Pura Apl*. **43 (2)** 101-12
[8] A. Márquez, C. Iemmi, J. Campos, M.J. Yzuel 2006 *Opt. Lett.* **31** 392-94
[9] M. S. Millán, J. Otón, E. Pérez-Cabré 2006 *Opt. Express*, **14** 6226-42
[10] M. S. Millán, J. Otón, E. Pérez-Cabré 2006 *Opt. Express*, **14** 9103-12
[11] Holoeye Photonics AG and Holoeye Corporation, http://www.holoeye.com
[12] J. Otón, P. Ambs, M. S. Millán, E. Pérez-Cabré 2007 *Appl. Optics* **46** 5667-79

Acknowledgments
This research was supported by Ministerio de Ciencia e Innovación and FEDER funds under project DPI2009-08879.

.